

Reduction of Spectral Ghost Artifacts in High-Resolution Echo-Planar Spectroscopic Imaging of Water and Fat Resonances

Weiliang Du,¹ Yiping P. Du,² Xiaobing Fan,¹ Marta A. Zamora,¹ and Gregory S. Karczmar^{1*}

Echo-planar spectroscopic imaging (EPSI) can be used for fast spectroscopic imaging of water and fat resonances at high resolution to improve structural and functional imaging. Because of the use of oscillating gradients during the free induction decay (FID), spectra obtained with EPSI are often degraded by Nyquist ghost artifacts arising from the inconsistency between the odd and even echoes. The presence of the spectral ghost lines causes errors in the evaluation of the true spectral lines, and this degrades images derived from high-resolution EPSI data. A technique is described for reducing the spectral ghost artifacts in EPSI of water and fat resonances, using echo shift and zero-order phase corrections. These corrections are applied during the data postprocessing. This technique is demonstrated with EPSI data acquired from human brains and breasts at 1.5 Tesla and from a water phantom at 4.7 Tesla. Experimental results indicate that the present approach significantly reduces the intensities of spectral ghosts. This technique is most useful in conjunction with high-resolution EPSI of water and fat resonances, but is less applicable to EPSI of metabolites due to the complexity of the spectra. Magn Reson Med 49:1113–1120, 2003. © 2003 Wiley-Liss, Inc.

Key words: artifact; odd and even echoes; echo-planar spectroscopic imaging; spectral ghost artifacts; high spectral and spatial resolution imaging

The desire to shorten imaging time has stimulated the use of fast alternating gradients in many MRI methods. Echo-planar spectroscopic imaging (EPSI) uses an alternating readout gradient for simultaneous encoding of the chemical shift dimension and one spatial dimension, and phase-encoding gradients for the other spatial dimensions. This strategy was first proposed by Mansfield (1) and has been successfully advanced by Posse et al. (2,3) and other workers for metabolite imaging (4–9), water and fat structural imaging (10–14), and functional imaging (3,15,16).

Compared to conventional phase-encoded spectroscopic imaging (SI), EPSI has the advantage of significantly reduced scan time; however, it places strong demands on the MR system, especially the gradient hardware. Inconsis-

tency (i.e., discontinuity in magnitude and phase) between the odd and even echoes often arises because of the use of the echo-planar gradients. This effect is well known in echo-planar imaging (EPI). In EPI, the inconsistency causes Nyquist image ghosts in the phase-encoding dimension, since the odd and even echoes represent interlaced phase-encoded lines in k -space (17). Because the odd and even echoes encode the spectral dimension in EPSI, the signal inconsistency causes Nyquist ghosts in resulting spectra. The spectral ghosts are detrimental in two ways. First, the ghost peak of one true peak may appear on top of or near a second true peak, impeding accurate quantification of the latter peak and altering the lineshape. Second, the intensity of the true peak is reduced because of the “energy leakage” from the true peak to the ghost peak. The spectral ghosts are especially problematic when EPSI is used for high spectral and spatial (HISS) imaging (10,11,16) where the goal is to obtain detailed water and fat spectra for anatomic and functional imaging.

A number of techniques have been proposed for the reduction of spectral ghost artifacts. One widely used and effective method is to separate the odd and even echoes in data processing (2,13,15). Unfortunately, this sacrifices half of the spectral bandwidth, which is already small in high spatial resolution EPSI. Alternatively, the odd and even echoes are combined for processing using the interlaced Fourier transform method (6) or the Fourier shift method (18). These techniques address the issue of non-uniform temporal sampling arising from the evolution of the free induction decay (FID) during each gradient echo. With these approaches, it is implicitly assumed that data are precisely sampled along a theoretically determined trajectory in k - t -space. In other words, the odd and even echoes are properly aligned and no corrections are made to the data at the center of k -space. In practice, this assumption is often invalid. Echo misalignments and distortions often lead to Nyquist ghosts in images obtained with EPI (17), and should be accounted for. Corrections for echo misalignment have been developed for EPSI by measuring the k - t trajectory and interpolating data at the desired locations (6,13). The main drawback of this method is the complicated procedure required for k - t trajectory measurement.

In this article, we present a new method to reduce the spectral ghost artifacts in EPSI by correcting the echo misalignment and phase discontinuities between the odd and even echoes. This approach is conceptually an extension of the echo shifting and phase correcting method that has been effective in removing inconsistency between the odd and even echoes for EPI data (17). The echo misalign-

¹Department of Radiology, University of Chicago, Chicago, Illinois.

²Department of Psychiatry and Radiology, University of Colorado Health Sciences Center, Denver, Colorado.

Grant sponsor: NCI; Grant numbers: RO1CA75476; RO1CA78803; Grant sponsor: Army Breast Cancer Research Program; Grant number: DAMD 17-99-1-9121; Grant sponsor: General Electric.

*Correspondence to: Gregory S. Karczmar, Ph.D., Department of Radiology, MC 2026, University of Chicago, 5841 S. Maryland Ave., Chicago, IL 60637. E-mail: gskarcm@midway.uchicago.edu

Received 8 October 2002; revised 13 January 2003; accepted 6 February 2003.

DOI 10.1002/mrm.10485

Published online in Wiley InterScience (www.interscience.wiley.com).

© 2003 Wiley-Liss, Inc.

ment is corrected by shifting the “centers of mass” (CM) of the odd and even echoes, and a zero-order phase correction is then applied to the odd echoes to minimize the spectral ghost intensity. This method takes advantage of the high SNR signals at the k -space center to measure inconsistencies in position and phase between the odd and even echoes. All corrections are made during data postprocessing, i.e., without the need for additional reference scans.

This technique has been applied to high spatial resolution EPSI data obtained from human brains and breasts at 1.5 Tesla, and from a water phantom at 4.7 Tesla. The MR images were acquired using an EPSI sequence without water or fat suppression. Water and fat spectra obtained with the present method and the conventional FFT method were compared to demonstrate the effectiveness of the new method.

MATERIALS AND METHODS

Data Acquisition

EPSI Pulse Sequence

The EPSI pulse sequence we implemented was a gradient-recalled multiecho sequence with 64 or 128 gradient echoes excited along the x dimension using trapezoidal readout gradients. The second spatial dimension (y) was provided by phase-encoding gradients between excitation and detection.

To provide sufficient spectral bandwidth, we collected the EPSI data in multiple (N_{int}) acquisitions. In each acquisition (or interleaf) the temporal offset of the echo train from the excitation pulse was incremented by Δt . This effectively reduced the time interval between adjacent gradient echoes (i.e., echo spacing, or $T_{\text{esp}} = N_{\text{int}}\Delta t$), and thus increased the spectral bandwidth by a factor of N_{int} .

Phantom Studies

Phantom experiments were performed on a 4.7 Tesla magnet (Omega; GE/Bruker, Fremont, CA). The phantom was a bottle of copper sulfate solution with an inner diameter of 24 mm. EPSI scans were performed through a 1-mm-thick axial slice with an in-plane resolution of $0.38 \times 0.38 \text{ mm}^2$ and a field of view (FOV) of 48 mm. The readout gradient consisted of 64 alternating lobes, each of which had two linear ramps (0.5 ms each) and a plateau (3.2 ms). Data were sampled only during the plateau phase of the gradient. The echo train lasted for 270 ms, yielding spectral resolution of 3.7 Hz. Interleaved EPSI datasets ($N_{\text{int}} = 2$) were acquired with an echo train offset of 2.1 ms so that the combination of the two interleaves resulted in a spectral bandwidth of 473 Hz. Each EPSI interleaf was acquired in 128 s ($\text{TR} = 1 \text{ s}$).

Human Studies

Healthy volunteers were imaged on a 1.5 Tesla MR scanner (Signa; GE Medical Systems, Milwaukee, WI), following a protocol approved by the University of Chicago Institutional Review Board. EPSI images were obtained in an axial slice through the brains ($N = 8$) or in a sagittal slice through the breasts ($N = 2$, female). Imaging parameters

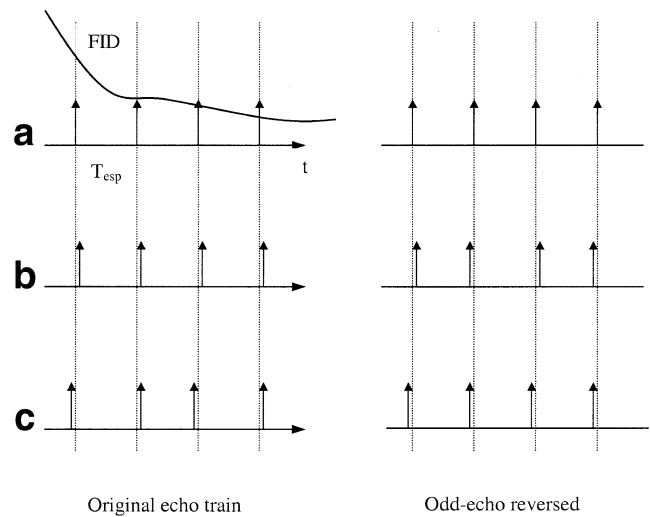


FIG. 1. Misalignment of the gradient echoes before (left) and after (right) the reversal of the odd echoes. The short arrows indicate the position of $k_x = 0$ point in each echo. **a:** Ideal alignments. **b:** A temporal shift of the entire echo train. **c:** Uneven spacing between adjacent echoes.

were: $\text{TR} = 500 \text{ ms}$, sampling bandwidth = $\pm 62.5 \text{ kHz}$, slice thickness = 4 mm, $\text{FOV} = 24 \text{ cm}$, spectral bandwidth = 333 Hz, matrix size = $256 (x) \times 256 (y) \times 128 (f)$, and $N_{\text{int}} = 1$. The EPSI scan was acquired in 128 s.

Postprocessing

Echo Misalignment

In an ideal EPSI experiment, the center of k -space (i.e., the $k_x = 0$ point) is traversed repeatedly with a constant time interval (Fig. 1a). Because of the opposite directions of the trajectories along k_x caused by the alternating readout gradients, the odd (or even) echoes must be reversed during data processing; however, the alignment of the $k_x = 0$ points does not change in the ideal situation. Two types of echo misalignments occur in practice due to various scanner- or sample-related imperfections. In the first type (Fig. 1b), the echo train is temporally shifted relative to the start of data acquisition, due to system timing errors, imperfection of gradient hardware (6,13), and uncompensated eddy currents (19,20). The reversal of the odd echoes translates this temporal shift in the echo train into a relative misplacement along k_x between the odd and even echoes. This misplacement generates spectral ghost artifacts when the echoes are used to produce spectra. In the second type of echo misalignment (Fig. 1c), the odd and even echoes are unevenly spaced within the echo train. This misalignment may be due to background gradients resulting from improper shimming, local susceptibility inhomogeneity, and eddy currents (21), or to an inaccurate dephasing gradient applied along k_x before the alternating readout gradients. As a result, the FID signals are not uniformly sampled at all k -space positions, including the $k_x = 0$ point, which introduces apparent magnitude and phase discontinuities between the odd and even samples, and thus generates spectral ghosts.

Echo Shift Correction

Previous EPSI studies either assumed an ideal echo misalignment (18) (i.e., no corrections are made to signals at k -space center) or corrected the first type of echo misalignment described above based on a predetermined k -space trajectory (6,13). In this study we corrected for the first type of echo misalignment by shifting the positions of the odd and even echoes using the information derived from the EPSI data itself. The raw data in the form of echo trains were grouped into a 3D signal matrix, $S(k_x, k_y, n)$, where n indexed the echoes (0, 1, 2, . . .) in the echo train and the odd echoes ($n = 1, 3, . . .$) were reversed. Then the k -space center ($k_x = 0, k_y = 0$) was approximated as the CM of the k -space signals for each echo, using the following formula:

$$CM_{k_x}(n) = \frac{\sum_{k_x, k_y} k_x \cdot |S(k_x, k_y, n)|}{\sum_{k_x, k_y} |S(k_x, k_y, n)|}$$

$$CM_{k_y}(n) = \frac{\sum_{k_x, k_y} k_y \cdot |S(k_x, k_y, n)|}{\sum_{k_x, k_y} |S(k_x, k_y, n)|}. \quad [1]$$

The differences between the CMs of the first five even echoes and the CMs of the immediately adjacent five odd echoes (after reversal of odd echoes) were calculated and averaged. These echoes were used because of their relatively high signal-to-noise ratio (SNR). Half of the averaged difference was used to shift the original echo train (i.e., before the odd echoes were reversed). Shifts that were smaller than one data point were performed using the Fourier shift theorem (i.e., data were Fourier transformed, a linear phase term was added, and then data were inversely Fourier transformed). The shifted echo train data were then regrouped into the matrix $S(k_x, k_y, n)$ for further processing.

Phase Correction

Echo misalignment of the second type described above led to nonuniform sampling of FID signals at all k -space points. Instead of assuming a uniform sampling at $k_x = 0$ and correcting the phases of the signals at other k -space points (6,18), we used a constant phase factor to correct for the phases of the odd echo signals at all k -space points. The phase factor was derived from the EPSI data itself, as follows:

1. For each echo n , the middle point (presumably, $k_x = k_y = 0$) of the signal matrix S was extracted. A function, named $FID_{k_{00}}(n)$, was formed with the extracted samples and was Fourier transformed. In the EPSI data from water phantom and human brains, two peaks arose in the resulting spectrum that were exactly half of the spectral bandwidth apart. The peak with larger magnitude was identified as the “true” water peak, while the other peak was regarded as the “ghost” peak. In the case of breast EPSI, the resulting spectrum often consisted of a relatively strong fat peak, a relatively strong water peak ~ 216 Hz away (~ 3.4 ppm) from the fat peak, and two smaller peaks

located half of the spectral bandwidth away from the fat peak and the water peak, respectively. We picked the peak with the largest magnitude (either the fat peak or the water peak) as the “true” peak, and the peak at half of spectral bandwidth away from this peak as the “ghost” peak.

2. The magnitudes of the true peak and the ghost peak were quantified as a summation of spectral intensities over a narrow neighborhood (e.g., 3–5 bins wide). Baseline was removed prior to the spectral summation, by subtracting a smoothed spectrum (boxcar length of ~ 15 bins) from the original spectrum. The ratio of the magnitude of the ghost peak to the magnitude of the true peak is herein referred to as the “ghost-to-true ratio” (GTR).

3. A phase angle ϕ was chosen from the range $(-\pi, \pi)$. A phase term $e^{-j2\pi\phi}$ was multiplied to the signals of the odd echoes at all k -space points. Steps 1 and 2 were repeated and the GTR was reevaluated.

4. The amount of phase correction was found using a Golden Section algorithm such that GTR was minimized.

Interleaved Acquisition

The correction methods described above were also extended to correct for the global phase changes in interleaved EPSI data. Each interleaf was treated separately with the echo shift and phase corrections described above. Then the interleaves were combined and a zero-order phase correction was applied to each interleaf (i.e., all echoes in that interleaf) except the first interleaf, in order to force the phase of every interleaf to be consistent with the first one. This zero-order phase correction was similar to the phase correction described above, except that the minimization problem in step (4) became multidimensional ($N_{\text{int}}-1$). An IDL (Research Systems, Boulder, CO) routine employing the Powell’s minimization algorithm was used in this task.

Method Evaluation

The EPSI spectrum in each pixel was obtained with a 3DFT following the echo shift and phase corrections. Images were formed with intensities proportional to the magnitude of the true peak, the magnitude of the ghost peak, and their ratio (GTR) using uncorrected and corrected spectra in each pixel. These variables were also reported quantitatively. To take the variation of these variables across the image into account, we pooled the measurements from all pixels with maximum spectral intensity 10 times above the noise level. Since these variables (e.g., GTR) did not necessarily follow a Gaussian distribution, we reported the median of pooled data along with the 20% and 80% quantiles as an estimate of the range of the measured variables.

RESULTS

Phantom

The CM calculated from the phantom EPSI data exhibits oscillatory displacements between the odd and even echoes in the readout (k_x) direction (Fig. 2a). Oscillation in CM is not seen in the phase-encoding (k_y) direction in the same EPSI data. Conventional phase-encoded SI (i.e., no

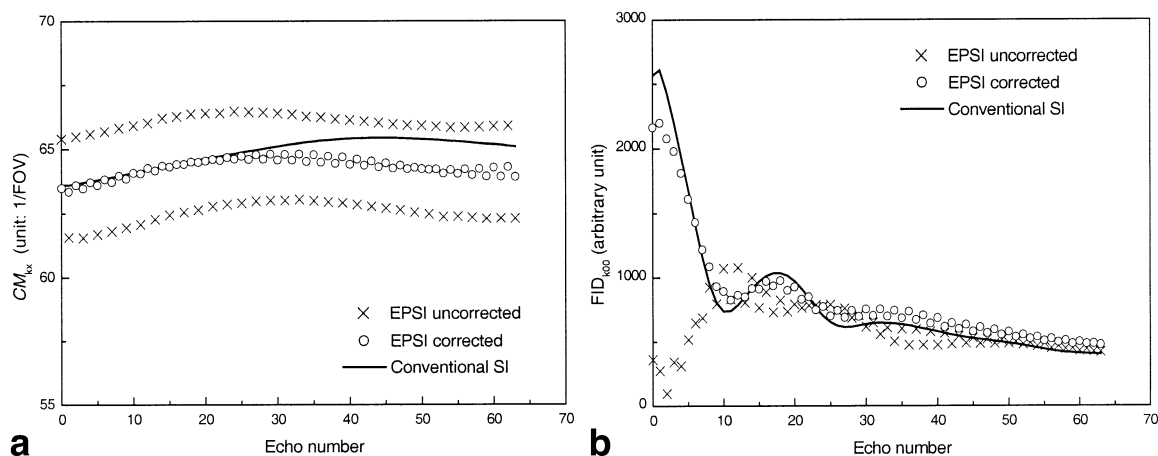


FIG. 2. Echo shift correction in EPSI data obtained from a water phantom. **a:** CM_{k_x} (defined in Methods) as a function of the index of the echoes in uncorrected EPSI (cross), EPSI with echo shift correction (circle), and conventional phase-encoded SI (solid line). **b:** The magnitude of $FID_{k_{00}}$ from uncorrected EPSI, corrected EPSI, and conventional SI.

readout gradients) of the same slice under the same shim conditions shows similar overall trends of CM shifts, but no oscillatory pattern in either the k_x or the k_y dimensions. This excludes the possibility that the relative echo shift in the readout direction (k_x) is due to the nature of the imaged object, or to off-resonance effects such as background gradients. The echo misalignment is evidently related to the alternating readout gradient and relevant data acquisition. A temporal offset ($66 \mu\text{s}$, or 2.65 data points) was used for the echo shift correction. As a result, the CM of the corrected EPSI data shows a reduced amplitude of oscillation and approaches the CM obtained with the conventional SI data (Fig. 2a). Also, the shape of the corrected $FID_{k_{00}}$ shows much better agreement with the $FID_{k_{00}}$ measured with the conventional SI (Fig. 2b).

For the first interleaf of the phantom EPSI data, the GTR was minimized with a phase correction of $\phi = 40.7^\circ$. For the second interleaf, the GTR was minimized with $\phi = 41.8^\circ$. To combine the two interleaves, a phase correction of 0° was found to be necessary to correct for all echoes from the second interleaf. Nonzero phase corrections were made to the interleaves in other EPSI scans (data not shown here).

The EPSI data were also reconstructed without echo shift and phase corrections. A true water peak and three

ghost peaks were found in the uncorrected spectra from most pixels. Figure 3 shows images synthesized from the peak height of the true water peak and the peak heights of the ghost peaks. Bright and dark streak patterns are evident in all uncorrected images. Where the signal intensity is strong in the ghost peaks (areas of hyperintensity in b, c, and d), the signal intensity is weak in the true water peak (areas of hypointensity in a). These artifacts are removed in the corrected peak height image (e). The intensities of the ghost peaks drop substantially (b vs. f, c vs. g, d vs. h) as the intensities of the true peaks increase (a vs. e), especially in pixels that originally had strong spectral ghosts. Table 1 summarizes the reduction of spectral ghosts in one- and two-interleaf EPSI datasets obtained with the water phantom.

Human Brain and Breast

Figure 4 demonstrates the effectiveness of the correction method on the EPSI data obtained from human brain. The ghost peaks are reduced to noise level in all pixels. The magnitudes of the true water peak increase nonuniformly across the image after the corrections. The increase is relatively large at locations where the spectral ghost is strong (near the edges of the brain). Table 2 shows the

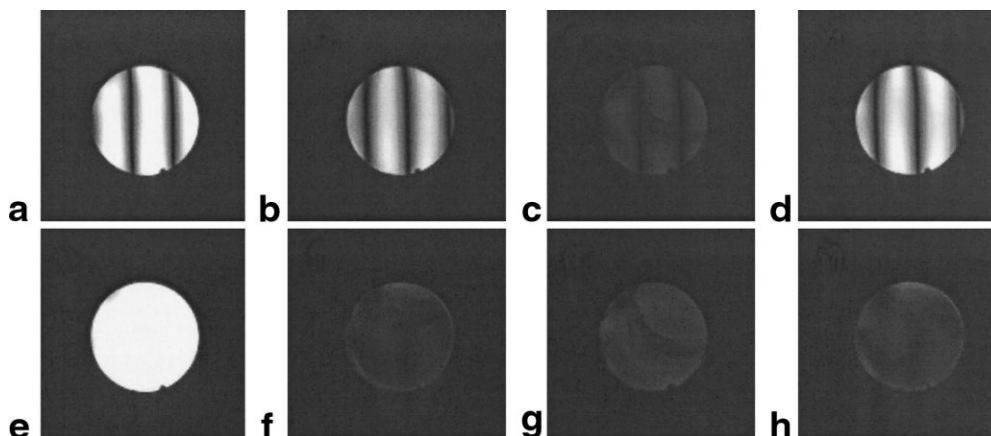


FIG. 3. Images synthesized from interleaved ($N_{\text{int}} = 2$) EPSI data without (upper panels) and with (lower panels) echo shift and phase corrections. From left to right, image intensity is proportional to the magnitude of the spectral peak at f_0 (a and e), $f_0 + bw/4$ (b and f), $f_0 + bw/2$ (c and g), and $f_0 + bw \cdot 3/4$ (d and h), where bw is the spectral bandwidth, f_0 is the frequency of the true water peak. The alternating readout gradient was applied in the horizontal direction.

Table 1
Reduction of the Spectral Ghost Peaks With the Echo Shift Correction and/or Phase Correction in EPSI Scans of a Water Phantom at 4.7 T*

	One-interleaf EPSI				Two-interleaf EPSI	
	Uncorrected	Echo shift correction only	Phase correction only	Echo shift and phase correction	Uncorrected	Echo shift and phase correction
Magnitude of true peak	3.40 (1.22, 5.01)	4.93 (4.76, 5.31)	3.46 (1.19, 5.13)	5.26 (5.09, 5.64)	4.31 (1.66, 6.22)	6.36 (6.17, 6.75)
Magnitude of ghost peak	3.65 (1.30, 5.15)	1.38 (1.11, 1.61)	3.63 (1.32, 5.08)	0.15 (0.06, 0.24)	2.14 (0.94, 2.84)	0.22 (0.17, 0.31)
Ghost-to-true ratio ^a	1.05 (0.25, 4.31)	0.28 (0.23, 0.32)	1.03 (0.25, 4.07)	0.027 (0.011, 0.046)	0.49 (0.15, 1.76)	0.035 (0.027, 0.048)

*The data presented are 50% (i.e., median) and 20%, 80% quantiles (in parenthesis) of the measurements obtained over an ROI covering most area of the phantom.

^aGhost-to-true ratio is defined as the ratio of magnitude of the ghost peak to the magnitude of the true water peak (also see Materials and Methods).

quantitative results of spectral ghost reduction. The EPSI datasets are corrected with an echo shift of approximately 0–7 μ s and a zero-order phase of approximately -4° to 2° . The median of GTR before correction ranges from 2.4%

(volunteer 5) to 27% (volunteer 2), with an average of approximately 12%. After the corrections, the median of GTR decreases to between 2% and 5%, with an average of 3.5%. The original GTRs are large in volunteers 2 and 4;

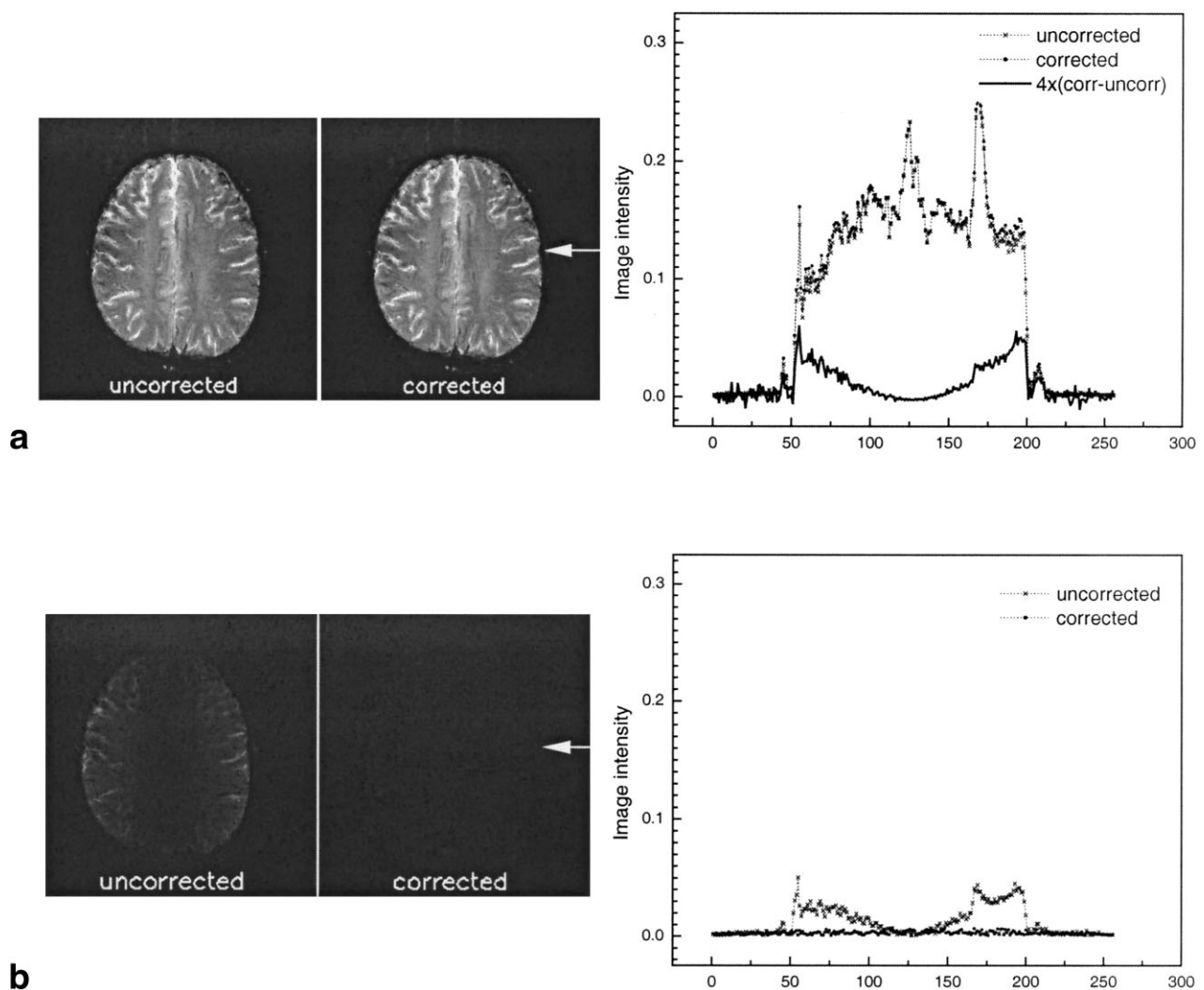


FIG. 4. Reduction of spectral ghosts in EPSI data of human brain. Image intensity is proportional to the magnitudes of the true water peak (a) or the ghost peak (b). All images are displayed with an identical windowing setting. On the right are profiles of the image intensities through a horizontal line indicated by the arrows.

Table 2
Echo Shift Correction, Zero-Order Phase Correction, and Reduction of Spectral Ghost Peaks in EPSI Scans of Normal Human Brains at 1.5T*

Volunteer	Echo train shift in time (μ s)	Phase correction on odd echoes (degree)	Ghost-to-true ratio	
			Uncorrected	Corrected
1	3.6	-0.34	0.099 (0.032, 0.204)	0.019 (0.012, 0.028)
2	6.0	-2.09	0.268 (0.093, 0.561)	0.041 (0.025, 0.065)
3	2.7	-3.46	0.095 (0.049, 0.191)	0.049 (0.034, 0.068)
4	6.7	-1.98	0.212 (0.077, 0.411)	0.035 (0.022, 0.065)
5	0.2	1.68	0.024 (0.013, 0.039)	0.027 (0.015, 0.041)
6	2.8	0.00	0.091 (0.049, 0.179)	0.047 (0.032, 0.065)
7	4.7	1.59	0.105 (0.041, 0.213)	0.036 (0.023, 0.054)
8	2.5	1.62	0.053 (0.029, 0.106)	0.028 (0.019, 0.040)

*The data presented are 50% (i.e., median) and 20%, 80% quantiles (in parenthesis) of the measurements obtained over an ROI covering most area of the brain.

therefore, the corrections are relatively large and lead to a remarkable decrease (sixfold) in the GTR. The original GTR is small in volunteer 5 and is not reduced after corrections.

The reduction of spectral ghosts in the EPSI data of human breast is illustrated in Fig. 5. In pixel 1 (which contains approximately equal amounts of fat and water tissues), the uncorrected spectrum clearly shows a ghost peak from the fat resonance and a weak ghost peak from the water resonance. In pixel 2 (which contains primarily fat), a single ghost peak is seen in the uncorrected spectrum. The magnitudes of the ghost peaks in these pixels are reduced to noise level after the corrections. Although spectra from many pixels in the breast, such as those shown in Fig. 5, were greatly improved by the correction, spectral ghosts in some pixels were not attenuated. Thus, the method in its current form is not as robust in the breast,

where fat and water signals are present, as it is in the brain, where only the water peak is significant.

DISCUSSION

In the present work, a method for reducing spectral ghosts in EPSI of water and fat resonances is demonstrated. This method uses the EPSI data from the center of k -space to correct the relative misplacement and zero-order phase difference between the odd and even echoes. In contrast to the commonly used technique that separates the odd and even echoes for image reconstruction, the present method removes the ghost peaks without reducing the spectral bandwidth to half. The savings on spectral bandwidth is particularly important for high spatial resolution EPSI applications, where the spectral bandwidth is usually limited by a relatively long duration of each gradient echo.

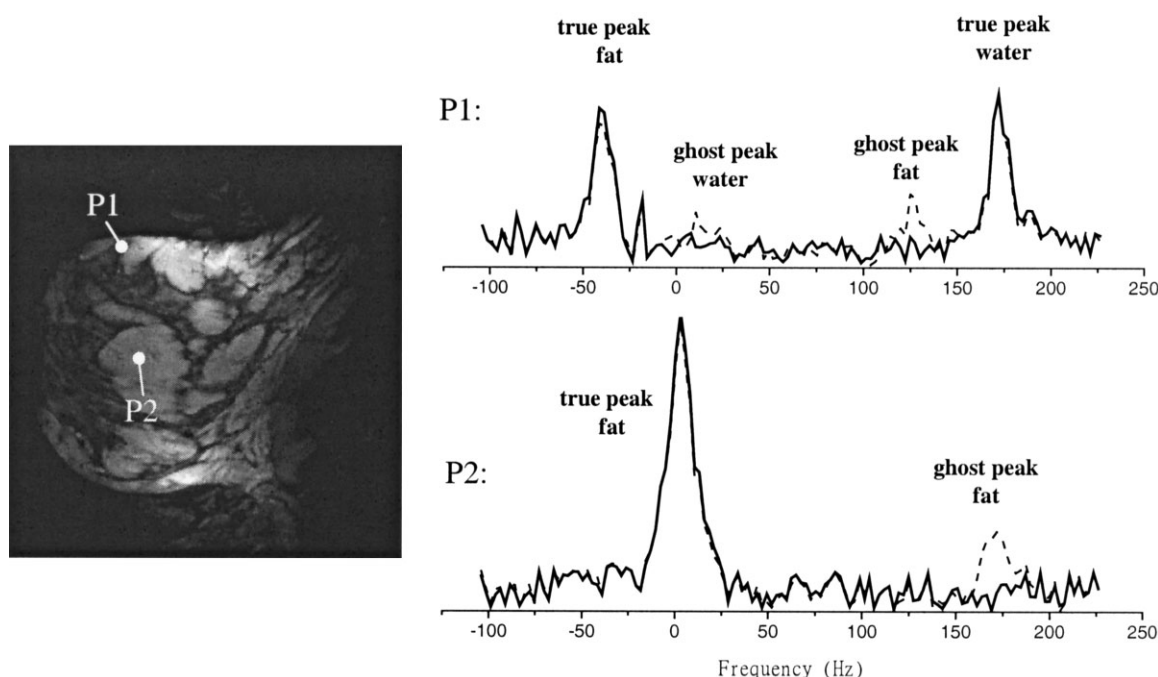


FIG. 5. Reduction of spectral ghosts in EPSI data of human breast. Left: An EPSI peak height image. Right: Spectra from two selected pixels (P1 and P2 in the image) calculated with (solid) and without (dash) echo shift and phase corrections.

Compared to other techniques that measure k -space trajectories to determine echo misalignments, the corrections are made during data processing, i.e., without the need for additional scans. This technique can be readily implemented with various EPSI sequences, such as 3D EPSI (9) and multishot EPSI (22).

EPSI data obtained without corrections display an interesting pattern of spectral ghost artifacts. The relative magnitudes of the ghost peaks vary significantly with respect to position in the echo-planar readout (x) direction, but do not vary as much in the phase-encoding direction (Figs. 3 and 4). The change in the ghost magnitude reflects a spatial variation in the extent of inconsistency between the odd and even echoes in the x direction, due to complicated echo shifts and distortions in the k_x direction. The inconsistency is severe at locations where large background gradients are present (e.g., near the edges of the brain in Fig. 4). Therefore, a global phase shift cannot by itself remove the artifacts from all pixels. In this work, the zero-order phase correction is used in combination with an echo shift correction. According to the Fourier theorems, an echo shift correction in the k_x direction is equivalent to a linear or first-order phase correction in the x direction. In essence, the echo shift correction is an extension of linear phase correction (17), which is widely used in EPI for removing image ghosts, to the task of removing spectral ghosts in EPSI. A nonlinear phase correction may better compensate for the effects of static field inhomogeneity on the data inconsistency, but it demands additional reference scans (17) and/or more sophisticated data processing techniques.

The zero-order phase correction is performed after the echo shift correction, i.e., after the linear phase discontinuity along the x direction is removed and only a residual constant phase discontinuity is left between the odd and even echoes. Despite its simplicity, the zero-order phase correction is effective: ghost intensity decreased from 0.28 to 0.027 in the water phantom experiments (see Table 1). The residual spectral ghosts are probably due to the fact that the phase evolution of the FID during each gradient echo is neglected in this study. During the echo-planar readout, the k_x - t -space is traversed in a zigzag fashion. Therefore, the sampling in time is not uniform for most of k -space points. This can generate spectral ghost artifacts. In the presence of a large off-resonance effect, it is necessary to make phase corrections for each k -space point (6,18). In our EPSI implementations for imaging water resonance in the phantom and human brains, the off-resonance effect is reasonably small. This is supported by the observation of the negligible magnitudes of residual ghost peaks after echo-shifting and phase correction (Fig. 4b). Further, the present method was also demonstrated to be useful for data acquired with interleaved EPSI. As with other multishot techniques (23,24), the signal varies from one acquisition to another. The zero-order phase correction provides a "self-navigated" way to trace and correct for the phase drift in the interleaved EPSI data.

The present method was developed for high-resolution functional and anatomic imaging of water and fat; therefore, it is more difficult to apply this method to water- and fat-suppressed EPSI of metabolites. First, the method may be sensitive to the noise in the data because of the low SNR

nature of metabolite imaging. Second, multiple chemical shifts change the signal patterns in k -space. As a result, the determination of the k -space center using the CM technique may not be accurate. Third, the ghost from one true line may overlap another true line. In this case, it becomes difficult to minimize the ghost intensity using the method described above. Finally, a constant phase correction that minimizes the ghost from one true line may not reduce the ghosts from other lines. Despite these limitations, the correction still works well on the high-resolution EPSI data obtained from human breast (Fig. 5). With the current implementation, the correction is applied directly to the water/fat EPSI data. For metabolite EPSI, it might be possible to calculate the amount of correction from a reference scan in which water signal is not suppressed. Then the correction could be applied to the metabolite EPSI data, assuming that the inconsistency between the odd and even echoes is accurately measured with the reference scan. This hypothesis was not validated in this work, and requires further investigation.

It is interesting to note that significantly larger echo shift and phase corrections are necessary for the EPSI data obtained at 4.7 T compared to 1.5 T. Thus, the correction is more beneficial for the 4.7 T data. This is probably because of a relatively better performance of echo-planar gradients and relatively smaller background gradients on the lower field. The results from EPSI measurements may be used to characterize the system inaccuracies and eddy-current effects for EPI applications (25,26). For example, the oscillatory pattern of the CM of the gradient echoes is a sensitive indicator of system timing errors (Fig. 2a). In addition, the linear or nonlinear trend in the CM may be used to guide adjustment of shims to reduce background gradients.

In conclusion, a new method for reducing spectral ghost artifacts in EPSI of water and fat resonances is presented. This method uses an echo shift and zero-order phase correction to remove the inconsistency between the odd and even echoes. The spectral ghost artifacts are reduced significantly, as demonstrated in phantom and in vivo EPSI of water and fat resonances at 1.5 T and 4.7 T. A further reduction of spectral ghosts in EPSI is expected when this technique is combined with other reconstruction strategies, such as nonlinear phase correction (17) and interleaved Fourier transform (6,18).

REFERENCES

1. Mansfield P. Spatial mapping of the chemical shift in NMR. *Magn Reson Med* 1984;1:370–386.
2. Posse S, Tedeschi G, Risinger R, Ogg R, Le Bihan D. High speed 1H spectroscopic imaging in human brain by echo planar spatial-spectral encoding. *Magn Reson Med* 1995;33:34–40.
3. Posse S, Dager SR, Richards TL, Yuan C, Ogg R, Artru AA, Muller-Gartner HW, Hayes C. In vivo measurement of regional brain metabolic response to hyperventilation using magnetic resonance: proton echo planar spectroscopic imaging (PEPSI). *Magn Reson Med* 1997;37:858–865.
4. Matsui S, Sekihara K, Kohno H. Spatially resolved NMR spectroscopy using phase-modulated spin-echo-trains. *J Magn Reson* 1986;67:476–490.
5. Webb P, Spielman D, Macovski A. A fast spectroscopic imaging method using a blipped phase encode gradient. *Magn Reson Med* 1989;12:306–315.

6. Metzger G, Hu X. Application of the interlaced Fourier transform to echo-planar spectroscopic imaging. *J Magn Reson* 1997;125:166–170.
7. Hyder F, Renken R, Rothman DL. In vivo carbon-edited detection with proton echo-planar spectroscopic imaging (ICED PEPSI): [3,4-(13)CH(2)]glutamate/glutamine tomography in rat brain. *Magn Reson Med* 1999;42:997–1003.
8. Richards TL, Corina D, Serafini S, Steury K, Echelard DR, Dager SR, Marro K, Abbott RD, Maravilla KR, Berninger VW. Effects of a phonologically driven treatment for dyslexia on lactate levels measured by proton MR spectroscopic imaging. *Am J Neuroradiol* 2000;21.
9. Ebel A, Soher BJ, Maudsley AA. Assessment of 3D proton MR echo-planar spectroscopic imaging using automated spectral analysis. *Magn Reson Med* 2001;46:1072–1078.
10. Du W, Du YP, Bick U, Fan X, MacEneaney PM, Zamora MA, Medved M, Karczmar GS. High spectral and spatial resolution MR imaging of breast—preliminary experience. *Radiology* 2002;224:577–585.
11. Kovar DA, Al-Hallaq HA, Zamora MA, River JN, Karczmar GS. Fast spectroscopic imaging of water and fat resonances to improve the quality of MR images. *Acad Radiol* 1998;5:269–275.
12. Kuroda K, Mulkern RV, Oshio K, Panych LP, Nakai T, Moriya T, Okuda S, Hynynen K, Joles FA. Temperature mapping using the water proton chemical shift: self-referenced method with echo-planar spectroscopic imaging. *Magn Reson Med* 2000;43:220–225.
13. Sarkar S, Heberlein K, Metzger GJ, Zhang X, Hu X. Applications of high-resolution echoplanar spectroscopic imaging for structural imaging. *J Magn Reson Imaging* 1999;10:1–7.
14. Yang QX, Demeure RJ, Dardzinski BJ, Arnold BW, Smith MB. Multiple echo frequency-domain image contrast: improved signal-to-noise ratio and T2 (T2*) weighting. *Magn Reson Med* 1999;41:423–428.
15. Barth M, Reichenbach JR, Venkatesan R, Moser E, Haacke EM. High-resolution, multiple gradient-echo functional MRI at 1.5 T. *Magn Reson Imaging* 1999;17:321–329.
16. Du YP, Du W, Uftring SJ, Fan X, Karczmar GS. fMRI with high spectral and spatial resolution echo-planar spectroscopic imaging at 1.5T. In: Proceedings of the 9th Annual Meeting of ISMRM, Glasgow, Scotland, 2001. p 1254.
17. Bruder H, Fischer H, Reinfelder HE, Schmitt F. Image reconstruction for echo planar imaging with nonequidistant *k*-space sampling. *Magn Reson Med* 1992;23:311–323.
18. Hanson LG, Schaumburg K, Paulson OB. Reconstruction strategy for echo planar spectroscopy and its application to partially undersampled imaging. *Magn Reson Med* 2000;44:412–417.
19. Takahashi A, Peters T. Compensation of multi-dimensional selective excitation pulses using measured *k*-space trajectories. *Magn Reson Med* 1995;34:446–456.
20. Haacke EM, Brown RW, Thompson MR, Venkatesan R. *Magnetic resonance imaging: physical principles and sequence design*. New York: John Wiley and Sons; 1999. p 846–848.
21. Jezzard P, Barnett AS, Pierpaoli C. Characterization of and correction for eddy current artifacts in echo planar diffusion imaging. *Magn Reson Med* 1998;39:801–812.
22. Tyszka JM, Mamelak AN. Volumetric multishot echo-planar spectroscopic imaging. *Magn Reson Med* 2001;46:219–227.
23. Hu X, Kim SG. Reduction of signal fluctuation in functional MRI using navigator echoes. *Magn Reson Med* 1994;31:495–503.
24. Glover GH, Lai S. Self-navigated spiral fMRI: interleaved vs. single-shot. *Magn Reson Med* 1998;39:361–368.
25. Chen NK, Wyrwicz AM. Correction for EPI distortions using multi-echo gradient-echo imaging. *Magn Reson Med* 1999;41:1206–1213.
26. Schmithorst VJ, Dardzinski BJ, Holland SK. Simultaneous correction of ghost and geometric distortion artifacts in EPI using a multiecho reference scan. *IEEE Trans Med Imaging* 2001;20:535–539.